Improved Green and Blue Fluorescent Proteins for Expression in Bacteria and Mammalian Cells[†,‡]

Gert-Jan Kremers,[§,||] Joachim Goedhart,[§] Dave J. van den Heuvel,[⊥] Hans C. Gerritsen,[⊥] and Theodorus W. J. Gadella, Jr.*[,§]

Section of Molecular Cytology and Centre for Advanced Microscopy, Swammerdam Institute for Life Sciences, University of Amsterdam, Kruislaan 316, 1098 SM Amsterdam, The Netherlands, and Department of Molecular Biophysics, Debye Institute, Utrecht University, P.O. Box 80000, 3508 TA Utrecht, The Netherlands

Received November 5, 2006; Revised Manuscript Received January 15, 2007

ABSTRACT: Fluorescent proteins have become an invaluable tool in cell biology. The green fluorescent protein variant EGFP is especially widely applied. Use of fluorescent proteins, including EGFP, however can be hindered by inefficient protein folding, resulting in protein aggregation and reduced fluorescence. This is especially profound in prokaryotic cells. Furthermore, EBFP, a blue fluorescent variant of EGFP, is rarely used because of its dim fluorescence and fast photobleaching. Thus, efforts to improve properties such as protein folding, fluorescence brightness, and photostability are important. Strongly enhanced green fluorescent (SGFP2) and strongly enhanced blue fluorescent (SBFP2) proteins were created, based on EGFP and EBFP, respectively. We used site-directed mutagenesis to introduce several mutations, which were recently shown to improve the fluorescent proteins EYFP and ECFP. SGFP2 and SBFP2 exhibit faster and more efficient protein folding and accelerated chromophore oxidation in vitro. For both strongly enhanced fluorescent proteins, the photostability was improved 2-fold and the quantum yield of SBFP2 was increased 3-fold. The improved folding efficiency reduced the extent of protein aggregation in *Escherichia coli*, thereby increasing the brightness of bacteria expressing SGFP2 7-fold compared to the brightness of those expressing EGFP. Bacteria expressing SBFP2 were 16-fold more fluorescent than those expressing EBFP. In mammalian cells, the improvements were less pronounced. Cells expressing SGFP2 were 1.7-fold brighter than those expressing EGFP, which was apparently due to more efficient protein expression and/or chromophore maturation. Mammalian cells expressing SBFP2 were 3.7-fold brighter than cells expressing EBFP. This increase in brightness closely resembled the increase in intrinsic brightness observed for the purified recombinant protein. The increased maturation efficiency and photostability of SGFP2 and SBFP2 facilitate detection and extend the maximum duration of fluorescence imaging.

After the first green fluorescent protein (GFP)[1] had been cloned from the jellyfish *Aequorea victoria* (*1*), a whole family of visible fluorescent proteins (VFPs) covering the visible spectrum from blue to (far) red has been isolated from various kinds of organisms (*2*, *3*). Nevertheless, the most frequently used fluorescent protein still is a modified version of *A. victoria* GFP, known as enhanced GFP (EGFP).

The excitation spectrum of wild-type GFP peaks at 395 nm with a secondary maximum at 475 nm. These two maxima arise from the protonated (395 nm) and deprotonated (475 nm) state of the chromophore. The emission spectrum of wild-type GFP exhibits a single emission maximum at 504 nm. In contrast, EGFP has only a single excitation maximum at 488 nm because of the S65T mutation that prevents chromophore protonation. The emission spectrum of EGFP closely resembles that of wild-type GFP. Furthermore, EGFP contains an F64L mutation and has a codon usage optimized for expression in mammalian cells. These features improve protein synthesis and increase the rate of chromophore formation (*4*−*6*).

Blue fluorescent proteins (BFPs) have been developed from GFP by substitution of tyrosine 66, located within the

[†] This work was supported by the European Union integrated project on Molecular Imaging (LSHG-CT-2003-503259). Part of this work was enabled via Vernieuwingsimpuls Grant 016.001.024 (T. den Blaauwen, University of Amsterdam) from the Netherlands Organization for Scientific Research (NWO).

[‡] The nucleotide sequences of all SVFP variants have been deposited in GenBank as accession numbers EF030489 (SGFP1), EF030490 (SGFP2), EF030491 [SGFP2(206A)], EF030492 [SGFP2(E222Q)], EF030493 [SGFP2(T65G)], EF030494 (SBFP1), and EF030495 (SBFP2).

* To whom correspondence should be addressed. Telephone: +31 20 525 6259. Fax: +31 20 525 7934. E-mail: Gadella@science.uva.nl.

[§] University of Amsterdam.

[||] Present address: Department of Molecular Physiology and Biophysics, Vanderbilt University Medical Center, 702 Light Hall, Nashville, TN 37232.

[⊥] Utrecht University.

[1] Abbreviations: AU, arbitrary units; BFP, blue fluorescent protein; CFP, cyan fluorescent protein; DIC, differential interference contrast; DTT, dithiothreitol; EBFP, enhanced blue fluorescent protein; EGFP, enhanced green fluorescent protein; EVFP, enhanced visible fluorescent protein; FLIM, fluorescence lifetime imaging microscopy; FRET, fluorescence resonance energy transfer; GFP, green fluorescent protein; GST, glutathione *S*-transferase; IPTG, isopropyl *β*-D-thiogalactopyranoside; OD, optical density; QY, fluorescence quantum yield; SVFP, strongly enhanced visible fluorescent protein; TCSPC, time-correlated single-photon counting; VFP, visible fluorescent protein; YFP, yellow fluorescent protein.

10.1021/bi0622874 CCC: $37.00
Published on Web 02/27/2007

chromophore for histidine (*7*). The Y66H mutation results in a blue-shifted fluorescence with excitation and emission maxima at 380 and 446 nm, respectively. BFPs are interesting because they can be used for multicolor imaging together with EGFP. BFPs, however, display weak fluorescence and suffer from fast photobleaching (*8*). Several attempts have been made to improve their fluorescence brightness. The brighter BFP variant P4-3 contains the additional Y145F point mutation, which increases the fluorescence quantum yield (QY) and accelerates chromophore formation (*9*). Furthermore, enhanced BFP (EBFP) has been developed by introducing mutations Y66H and Y145F into EGFP, resulting in a blue fluorescent protein with mammalian optimized codon usage (*10*). EBFP has a higher extinction coefficient and becomes more fluorescent in mammalian cells than P4-3. EBFP nonetheless still has a relative low QY and is therefore weakly fluorescent. In addition, EBFP remains very sensitive to photobleaching.

Numerous mutations that enhance the fluorescence brightness of *A. victoria* GFP-derived fluorescent proteins have been reported. These mutations act by improving, for example, chromophore formation (F64L), protein folding (S72A, V163A, and S175G), and solubility (M153T and V163A) or abolishing the tendency to dimerize (A206K) (*4*, *5*, *11*−*14*). Most of these mutations were found independently by random mutagenesis of GFP. Recently, introduction of the combined S72A, M153T, V163A, S175G, and A206K mutations has been shown to improve the protein folding and fluorescence brightness of EYFP and ECFP (*15*, *16*). In the study presented here, we describe the results of a similar strategy for developing improved green and blue fluorescent protein variants. In line with the previously described SYFP and SCFP variants, we named these improved fluorescent proteins SGFPs and SBFPs to indicate the upgrade from the well-known enhanced fluorescent proteins EGFP and EBFP.

EXPERIMENTAL PROCEDURES

Construction of Plasmid Vectors. SVFP variants were obtained by multiple rounds of site-directed mutagenesis on the yellow fluorescent protein variant Venus as described previously (*15*). A list of oligonucleotides used for mutagenesis is shown in Table S1 of the Supporting Information. For bacterial expression, all VFP variants were cloned into pGEX-MCS to produce glutathione *S*-transferase (GST)-tagged fusion proteins. SGFP2(E222Q) was cloned into pRSETb (Invitrogen, Breda, The Netherlands) to produce His_6-tagged protein. Mammalian expression vectors were created by exchanging EGFP from plasmid pEGFP-C1 (Clontech, Palo Alto, CA) for the VFP variants. All vectors were checked by DNA sequencing.

To obtain SGFP2-cyt, a nuclear export sequence was fused to the C-terminus of SGFP2. To create mCherry-nuc, a sequence encoding a polybasic stretch of amino acids was fused to the C-terminus of mCherry (*17*). SCFP3A-golgi was made by fusion of the pleckstrin homology domain of oxysterol binding protein (PH-OSBP) (*18*) to the C-terminus of SCFP3A (*15*). A nuclear export sequence was used as a linker between SCFP3A and PH-OSBP. mVenus-pm consisted of the PH domain of phospholipaseC-delta1 (*19*, *20*) fused to the C-terminus of mVenus.

Fluorescent Protein Isolation. Fluorescent proteins were isolated from *Escherichia coli* strain BL21(DE3) as described previously (*15*). After protein expression for 5 h at room temperature, fluorescent proteins were purified using glutathione-bound agarose (Sigma-Aldrich, St. Louis, MO) for GST-tagged proteins and His-bind Resin (Novagen, Darmstadt, Germany) for His_6-tagged proteins. Protein concentrations of all fluorescent fractions were determined with the Pierce BCA protein assay (Pierce Biotechnology, Rockford, IL), using a bovine serum albumin standard as a reference. Sample purity was checked by SDS−PAGE.

Protein Characterization. Spectral measurements were taken in 20 mM Tris-HCl and 1 mM EDTA (pH 8). Absorbance spectra were measured on a Uvikon293 dual-beam spectrophotometer (Bio-Tek Instruments, Winooski, VT). Extinction coefficients were calculated by applying Beer's law to the absorbance spectra of at least three independent protein samples ($0.1 < OD < 1$). Fluorescence spectra were measured on a PTI QuantaMaster 2000-4 fluorescence spectrofluorometer (Photon Technology International, Lawrenceville, NJ) and corrected for differences in excitation intensity and detector sensitivity. Quantum yields were determined for diluted VFP solutions from three independent protein isolations with a similar optical density ($OD \leq 0.05$). For GFP variants, fluorescein (Molecular Probes, Eugene, OR) in a borate buffer solution (pH 9.1) (QY 0.92) (*21*) was used as a quantum yield standard and for BFP variants quinine sulfate in 50 mM H_2SO_4 (QY 0.51, Fluka/Sigma-Aldrich, Zwijndrecht, The Netherlands). For pH titrations, fluorescent protein was diluted to 25−75 nM in 96-well plates containing 200 μL of titration buffer ranging from pH 3 to 10 (*15*). Plates were analyzed using a FL600 fluorescence microtiterplate reader (Bio-Tek Instruments) equipped with custom-ordered filters. For GFP and BFP fluorescence, BP485/20 and BP360/40 excitation filters and BP530/25 and BP460/40 emission filters (Chroma Technology Corp., Rockinham, VT) were used, respectively. The pK_a was determined by fitting the data to the Henderson−Hasselbalch equation.

Bleach Measurements. Microdroplets containing ~0.25 μM fluorescent protein [20 mM Tris-HCl, 1 mM EDTA, and 5% (v/v) polyethylene glycol 4000 (pH 8)] were created as an emulsion in 1-octanol as described previously (*15*). Single microdroplets were bleached under continuous widefield illumination on an Axiovert200M microscope (Zeiss, Jena, Germany) fitted with a Zeiss plan Neofluar 40 × 1.3 NA oil-immersion objective using a 100 W high-pressure mercury lamp for excitation. Bleach series were recorded with a Coolsnap HQ CCD camera (Roper Scientific, Tucson, AZ). GFP or BFP fluorescence was detected using HQ470/40 and D365/10 excitation filters, a Q495LP dichroic mirror, a 20/80 beam splitter, and HQ515/30 and GG400LP emission filters, respectively (Chroma Technology Corp.). Data analysis was done by curve fitting a single-exponential decay to the mean fluorescence over time.

Refolding and Oxidation of Fluorescent Proteins. Fluorescent protein was denatured by being heated for 5 min at 95 °C in 8 M urea and 1 mM DTT. For chromophore reduction, 5 mM sodium dithionite was present during denaturation. Refolding was initiated by 100-fold dilution in refolding buffer [50 mM Tris-HCl, 35 mM KCl, 2 mM $MgCl_2$, and 1 mM DTT (pH 7.5)] at 37 °C. Fluorescence recovery was normalized to the fluorescence intensity of an equal amount of native protein. Rate constants for refolding

and oxidation were obtained by fitting the data to a double-exponential equation (*15*).

Localization in E. coli. Protein expression was induced with 0.1 mM IPTG for 4 h at 37 °C. Bacteria were fixed with 2.8% formaldehyde and 0.04% glutaraldehyde and prepared for microscopy as described previously (*15*). Images were recorded with a Coolsnap FX CCD camera (Roper Scientific) connected to an Olympus BX60 fluorescence microscope (Japan) fitted with an Olympus U Plan Fl 100 × 1.3 NA oil-immersion phase contrast objective. GFP or BFP fluorescence was detected, as described in Bleach Measurements.

Relative Brightness in E. coli. Bacteria were grown to OD_{600} of ≈0.6 as described above. Cultures were diluted to an OD_{600} of 0.1 in triplicate and used to inoculate wells of flat bottom 96-well plates (Greiner Bio-One, Frickenhausen, Germany) in quadruplicate. Per well, 180 μL of medium containing 0.1 mM IPTG was inoculated with 20 μL of diluted bacteria. Bacteria were grown at 37 °C in the fluorescence microtiterplate reader while being shaken. Fluorescence was measured every 5 min using the filter sets as described for the pH titrations.

Transient Transfection of Mammalian Cells. Cells growing on glass coverslips (Ø = 24 mm) were transfected with 0.2−0.4 μg of plasmid DNA using 1.5 μL of Lipofectamine2000 (Invitrogen). Cells were used for experiments 16−24 h after transfection.

Flow Cytometry. HeLa cells transfected with equal amounts of DNA were analyzed by flow cytometry on a LSRII cytometer (Becton Dickinson, San Jose, CA). GFP fluorescence was excited at 488 nm and collected through a 530/30 nm bandpass filter. BFP fluorescence was measured using a 407 nm diode laser for excitation and a 440/40 bandpass filter.

Fluorescence Lifetime Imaging (FLIM). For frequency domain wide field FLIM measurements, the FLIM setup as described by ref *22* was used. For imaging of GFP, an argon laser (488 nm, 150 mW) (Melles-Griot, Carlsbad, CA), a Q495LP dichroic mirror, and a HQ515/30 bandpass emission filter (Chroma Technology Corp.) were used. FLIM stacks of 12 phase images were acquired with an exposure time of 250−1000 ms per image depending on the brightness of the samples, using a Zeiss plan Neofluar 40 × 1.3 NA oil-immersion objective. To minimize artifacts due to photobleaching, a permutated recording sequence was used (*23*).

Fluorescence decay curves were recorded using time-correlated single-photon counting (TCSPC) on a Nikon C1 confocal microscope (Nikon) equipped with a TimeHarp TCSPC board (PicoQuant GmbH). A 405 nm pulsed picosecond diode laser (PicoQuant GmbH) was used to excite the sample. Emission was selected using a 414 nm dichroic mirror and emission filters (420 nm long-pass and 460/50 nm bandpass filter) and detected with a GaAsP photocathode photon-counting PMT (Hamamatsu). The fluorescence lifetimes were determined from the TCSPC decay curves by fitting the curves to a sum of exponential functions using a nonlinear least-squares Levenberg−Marquardt fit algorithm (*24*). In the fitting procedure, the measured system time response was taken into account.

Confocal Microscopy. For microscopy, the cells were placed in extracellular-like buffer [140 mM NaCl, 5 mM KCl, 1 mM $CaCl_2$, 1 mM $MgCl_2$, 10 mM glucose, and 20 mM Hepes (pH 7.4)]. Confocal microscopy was performed on a Zeiss LSM510 confocal laser scanning microscope implemented on an inverted microscope (Axiovert 100, Zeiss) and fitted with a Plan-Neofluar 40 × 1.3 NA oil-immersion objective. Excitation was provided by two argon lasers (364 nm or 458, 488, and 514 nm) and a HeNe laser (543 nm). One primary dichroic mirror (HFT) and three secondary dichroic mirrors (NFT1−3) were used to separate excitation from emission and to direct fluorescence into different detector channels (Ch1−3). The light path in the microscope was as follows. The excitation light is reflected onto the sample by the HFT. Fluorescence from the sample passes the HFT and is split by NFT1. Light that is reflected by NFT1 is split once more by NFT2. Light reflected by NFT2 is filtered and detected in Ch1, and transmitted light is filtered and detected in Ch2. Light that is passed by NFT1 is split by NFT3. Light transmitted by NFT3 is filtered and detected in Ch3. Images with minimal cross-talk were aquired by operating in multitracking mode. For three-color imaging of SBFP2, SGFP2, and mCherry, the following settings were used: HFT UV/488/543/633, NFT1 545, NFT2 490, NFT3 635. SBFP2, SGFP2, and mCherry were excited at 364, 488, and 543 nm, and fluorescence was collected through BP385−470 (Ch1), BP505−530 (Ch2), and LP585 (Ch3) emission filters, respectively. For four-color imaging of SBFP2, SCFP3A, mVenus, and mCherry, the same settings that are described above were used for SBFP2 and mCherry, except that mCherry fluorescence was collected through an LP650 emission filter. For imaging SCFP3A and mVenus, HFT was changed to 458 and 514 nm and NFT2 to 515 nm. SCFP3A and mVenus were excited at 458 and 514 nm, and fluorescence was collected through BP470−500 (Ch1) and BP540/20 (Ch2) emission filters, respectively.

Table 1: Overview of Mutations in GFP and BFP Variants[a]

	mutations
EGFP	F64L, S65T
SGFP1	F64L, S65T, V68L, S72A, M153T, V163A, S175G, A206K
SGFP2	F64L, S65T, S72A, M153T, V163A, S175G, A206K
SGFP2(206A)	F64L, S65T, S72A, M153T, V163A, S175G
SGFP2(E222Q)	F64L, S65T, S72A, M153T, V163A, S175G, A206K, E222Q
SGFP2(T65G)	F64L, S65G, S72A, M153T, V163A, S175G, A206K
EBFP	F64L, S65T, Y66H, Y145F
SBFP1	F64L, Y66H, V68L, S72A, Y145F, M153T, V163A, S175G, A206K
SBFP2	F64L, Y66H, S72A, Y145F, M153T, V163A, S175G, A206K

[a] Annotation based on the wild-type GFP amino acid sequence [GenBank accession number M62653 (*1*)].

RESULTS

Construction of Novel GFP and BFP Variants. Optimized GFP and BFP variants were created by converting Venus, a recently described optimized folding variant of YFP (*16*), into green and blue fluorescent proteins. First, SGFP1 and SBFP1 were developed (Table 1). SGFP1 and SBFP1 still contained the V68L mutation which is not considered one of the folding mutations but rather a remnant of Venus and EYFP. Leucine 68 was therefore changed back to valine to create SGFP2 and SBFP2. In addition, the S65T mutation was removed from SBFP1 and SBFP2 since it was not present in BFP variant P4-3.

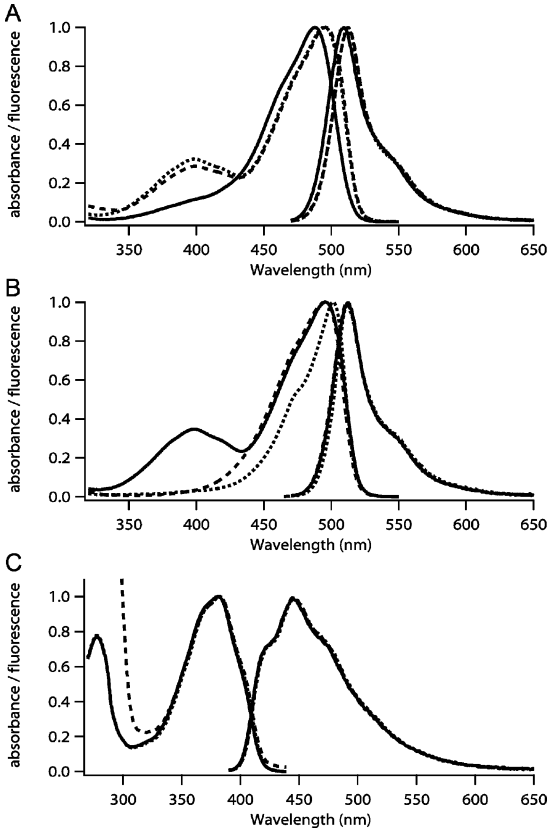

FIGURE 1: Normalized absorbance and fluorescence emission spectra of purified proteins. (A) Spectra of EGFP (—), SGFP1 (- - -), and SGFP2 (•••). (B) Spectra of SGFP2(206A) (—), SGFP2-(E222Q) (- - -), and SGFP2(T65G) (•••). (C) Spectra of EBFP (—), SBFP1 (- - -), and SBFP2 (•••). Emission spectra of GFP and BFP variants were recorded with excitation at 460 and 380 nm, respectively.

Spectral Characterization of GFP and BFP Variants. The absorbance of SGFP1 and SGFP2 peaked at 495 nm which was shifted to the red by 7 nm compared to that of EGFP (Figure 1A). Furthermore, a secondary absorbance maximum was observed at 398 nm, indicating chromophore protonation. To prevent chromophore protonation, additional mutagenesis was preformed on SGFP2 (Table 1). Chromophore protonation was effectively abolished by E222Q and T65G mutations. The absorbance spectrum of SGFP2(E222Q) was identical to that of SGFP2 except for the absorbance at 398 nm, whereas for SGFP2(T65G), the absorbance maximum was shifted to 501 nm and the shape of the absorbance spectrum resembled closely that of yellow fluorescent proteins (Figure 1B). Despite the changed absorbance spectra, the emission spectra of all GFP variants were remarkably similar, and the only difference was a small shift in the emission maxima of all SGFP variants (512 nm) (Table 2).

The molar extinction coefficient of SGFP1 and SGFP2 decreased compared to that of EGFP (Table 2). This decrease correlated with the extent of chromophore protonation. For SGFP2(E222Q), the molar extinction coefficient was similar to that of EGFP (Table 2). The T65G mutation on the other hand increased the molar extinction coefficient of SGFP2-(T65G) to 90 000 M^{-1} cm^{-1}. The QY of SGFP1 and SGFP2 ranged between 0.62 and 0.70, which was comparable to that of EGFP (0.65) (Table 2). In contrast, the QY of SGFP2-(T65G) was only 0.35, thereby counteracting the increased molar extinction coefficient. On the basis of the spectroscopic properties, SGFP2 was the brightest SGFP variant despite the partial chromophore protonation. The intrinsic brightness (i.e., the product of molar extinction coefficient and QY) of SGFP2, however, was lower than that for EGFP.

For the blue fluorescent proteins, the absorbance and emission spectra were similar, except for the high absorbance of SBFP1 around 280 nm (Figure 1C). The molar extinction coefficients of EBFP and SBFP2 (Table 2) were comparable, whereas for SBFP1, the molar extinction coefficient was severely reduced. This was caused by the presence of denatured protein after purification, as identified by SDS−PAGE (data not shown). The contribution of denatured protein also explained the high absorbance of SBFP1 at 280 nm. Remarkably, the QY of SBFP2 (0.47) was increased 3-fold compared to that of EBFP (0.15). For SBFP2, the intrinsic brightness was therefore approximately 3.5-fold higher than that for EBFP.

pK_a Measurements. The fluorescence intensity of VFPs is decreased at a reduced pH. To minimize the effects on VFP fluorescence as a result of changes in the intracellular pH, pK_a values well below physiological pH are recommended. The pK_a values of the SGFP variants were well below the physiological pH, ranging from 5.9 to 6.0 (Table 2), except for SGFP2(T65G), for which an increase in pK_a (6.7) was observed. Furthermore, for the blue fluorescent variants, the pK_a of SBFP2 was nearly 1 unit lower compared to that of EBFP (5.5 and 6.3, respectively).

Bleach Rates. Photobleaching is a major restriction for the application of fluorescent proteins. Use of EBFP especially has been limited because of its sensitivity to bleaching. Bleaching of microdroplets containing purified protein showed that SBFP1 bleached 3 times faster than EBFP. The photostability of SBFP2 on the other hand was 2-fold higher than that of EBFP (Table 2). A similar increase in photostability was observed for SGFP2 (Table 2). Hence, SGFP2 and SBFP2 were both more photostable than their established variants.

Protein Folding and Chromophore Oxidation. Introduction of folding mutations has been shown to enhance protein folding of cyan and yellow fluorescent proteins (*15*, *16*). Analogous to those results, the rate and efficiency of protein refolding of SGFP2 (1.84×10^{-2} s^{-1}; ~35%) were improved compared to those of EGFP (0.87×10^{-2} s^{-1}; ~20%), although refolding of SGFP1 was fastest and most efficient (3.15×10^{-2} s^{-1}; ~60%) (Figure 2 and Table 2). Furthermore, chromophore oxidation was accelerated several-fold for the SGFP variants ($3.4-5.1 \times 10^{-4}$ s^{-1}) compared to EGFP (1.3×10^{-4} s^{-1}). Only for SGFP2(E222Q) was the rate of oxidation reduced 10-fold. Refolding of SBFP2 was improved over that of EBFP, and the changes resembled those for SGFP2. For SBFP2, the rate of chromophore oxidation was 1.7×10^{-4} s^{-1}; however, we were unable to determine the rate of chromophore oxidation for EBFP because no fluorescence recovery was observed after chromophore reduction.

Localization in E. coli. Folding of VFPs in *E. coli* at 37 °C can be inefficient, resulting in a large amount of misfolded protein (*4*, *25*, *26*). Bacteria expressing EGFP and EBFP as GST fusion proteins became barely fluorescent, and fluorescence was observed almost exclusively in large fluorescent spots at the poles of the bacteria (Figure 3A,E). These spots were identified as aggregates or inclusion bodies

Table 2: Spectroscopic Characterization of GFP and BFP Variants

	ϵ^a ($\times 10^3$ M^{-1} cm^{-1})	QY[b]	pK_a	brightness[c] $\epsilon \times$ QY	brightness[c] *E. coli*	brightness[c] HeLa	τ_{bleach}[d]	K_{fold} ($\times 10^{-2}$ s^{-1})	K_{ox} ($\times 10^{-4}$ s^{-1})
EGFP	63 (488)	0.65 (509)	5.8	1	1	1	1	0.87	1.3
SGFP1	42 (495)	0.62 (512)	6.0	0.6	3.5	1.3	1.7	3.15	5.1
SGFP2	46 (495)	0.70 (512)	5.9	0.8	7.3	1.7	1.9	1.84	4.3
SGFP2(206A)	44 (496)	0.69 (512)	6.0	0.7	5.8	1.6	2.1	1.68	3.4
SGFP2(E222Q)	67 (496)	0.52 (512)	6.0	0.8	3.8		1.2	1.43	0.4
SGFP2(T65G)	90 (501)	0.35 (512)	6.7	0.6	1.6	1.2	1.0	1.50	5.0
EBFP	31 (380)	0.15 (446)	6.3	1	1	1	1	0.75	
SBFP1	2.3 (380)	0.40 (446)		0.2	0.6		0.3		
SBFP2	34 (380)	0.47 (446)	5.5	3.5	16.4	3.7	2.1	2.56	1.7
literature[e]									
EGFP	55−57 (488)	0.60 (509−511)	6					0.24	1.5
P4-3	14−22.3 (381)	0.30−0.38 (445)							
EBFP	31 (380)	0.17−0.25 (450)	5.8						

[a] Extinction coefficient with the absorbance maximum (nanometers) in parentheses. [b] Quantum yield with the emission maximum (nanometers) in parentheses. [c] Brightness determined as the intrinsic brightness of the purified protein ($\epsilon \times$ QY) and upon expression in *E. coli* and HeLa cells, relative to EGFP and EBFP, respectively. The intrinsic brightness of the GFP variants is corrected for the excitation efficiency at 488 nm. [d] Time needed to bleach 1/e of total fluorescence relative to EGFP or EBFP (higher numbers reflect a higher photostability). [e] Cited literature on EGFP (*5*, *6*, *11*, *39*, *40*), P4-3 (*9*−*11*), and EBFP (*5*, *10*, *39*).

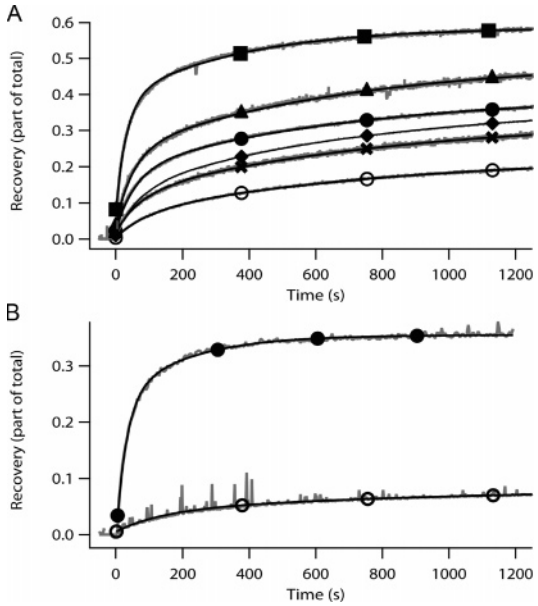

FIGURE 2: In vitro refolding of urea-denatured protein. (A) Fluorescence recovery of EGFP (○), SGFP1 (■), SGFP2 (●), SGFP2(206A) (▲), SGFP2(E222Q) (◆), and SGFP2(T65G) (×). (B) Fluorescence recovery of EBFP (○) and SBFP2 (●). The recovery is relative to the fluorescence of an equal amount of native protein. Traces and curve fits are representative curves of three individual experiments.

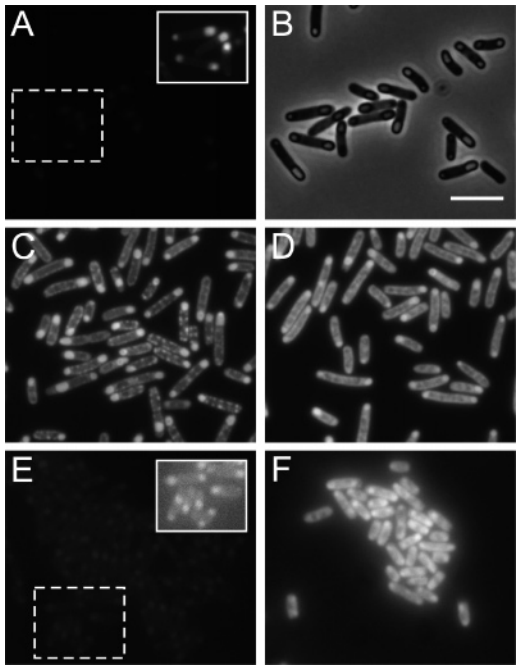

FIGURE 3: Localization of GST-tagged VFP variants in *E. coli*. Fluorescence micrographs of bacteria expressing GST-tagged EGFP (A), SGFP2(206A) (C), SGFP2 (D), EBFP (E), and SBFP2 (F). (B) Phase-contrast micrograph of panel A. Exposure times for fluorescence micrographs of the GFP and BFP variants were 15 and 750 ms, respectively. Insets in panels A and E show contrast-enhanced images of the dashed regions of interest. The scale bar is 2 μm.

by phase-contrast microscopy (Figure 3B). In contrast, bacteria expressing most SVFP variants became brightly fluorescent. SGFP2(206A), containing all folding mutations except A206K, accumulated in inclusion bodies at the poles of the cells but was also found in numerous small fluorescent spots throughout the cells (Figure 3C). SGFP2 was distributed most homogeneously throughout the bacteria (Figure 3D), although some aggregation remained at the poles of most cells. A similar localization pattern was observed for SBFP2 (Figure 3F). After protein induction for 4 h, SBFP1 fluorescence could not be detected above autofluorescence (data not shown).

Relative Brightness in E. coli. To study protein folding in living cells, we monitored the development of fluorescence upon expression of GST-tagged VFP variants in *E. coli*. Figure 4A exhibits an increased fluorescence for all bacteria expressing SGFP variants. *E. coli* expressing SGFP2 were most fluorescent and became 7.3-fold brighter than bacteria expressing EGFP (Table 2). Bacteria expressing SGFP1 were only half as bright as those expressing SGFP2, and fluorescence development was delayed. The largest increase in fluorescence brightness was observed for *E. coli* expressing SBFP2, which became 16-fold more fluorescent than bacteria expressing EBFP (Figure 4B and Table 2). In contrast, only after a prolonged time could SBFP1 fluorescence be detected above the level of autofluorescence, and bacteria expressing SBFP1 remained less bright than those expressing EBFP.

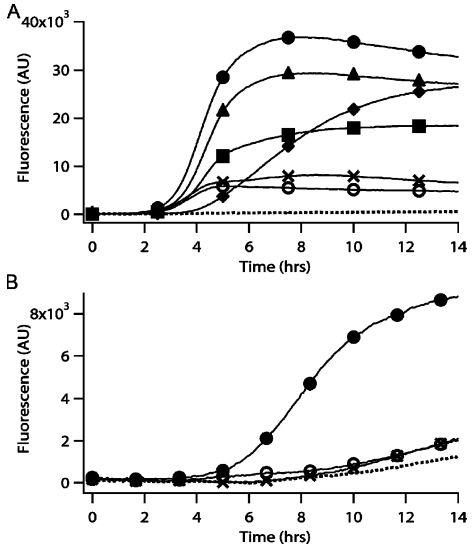

FIGURE 4: Time course of fluorescence development during VFP expression in *E. coli*. (A) Fluorescence development of bacteria expressing GST-tagged EGFP (○), SGFP1 (■), SGFP2 (●), SGFP2(206A) (▲), SGFP2(E222Q) (◆), and SGFP2(T65G) (×). (B) Fluorescence development of bacteria expressing GST-tagged EBFP (○), SBFP1 (×), and SBFP2 (●). Dotted lines (•••) indicate the autofluorescence of nontransformed bacteria. Traces represent the average of 12 independent growing *E. coli* cultures. Standard deviations fall within the symbols. Bacteria were incubated at 37 °C, and protein expression was initiated at time zero.

Relative Brightness in HeLa Cells. The relative brightness of HeLa cells expressing VFP variants was measured by flow cytometry. The relative brightness of all HeLa cells expressing SGFP variants was higher than for cells expressing EGFP (Table 2). Cells expressing SGFP2 were the brightest and became 1.7-fold more fluorescent than cells expressing EGFP. The relative brightness of HeLa cells expressing SGFP variants was 2-fold higher than the value expected on the basis of the intrinsic brightness determined for the purified VFPs. Cells expressing SBFP2 became 3.7-fold brighter than those expressing EBFP which is similar to the increase in intrinsic brightness of the purified protein.

Fluorescence Lifetime Imaging of GFP and BFP Variants. Fluorescence lifetime imaging (FLIM) of fluorescent proteins is a powerful technique for sampling the environment inside living cells, especially when using FRET applications to study protein interactions (*27*−*31*). We measured the fluorescence lifetimes (τ_φ and τ_m) of all GFP variants expressed in Swiss 3T3 cells using frequency domain FLIM (*22*). For all GFP variants except SGFP2(E222Q), τ_φ and τ_m were very similar (Table 3), indicating a nearly monoexponential fluorescence decay. The fluorescence lifetimes correlated well with the QY determined for purified recombinant protein. Interestingly, the slightly higher QY of SGFP2 was accompanied by a significant increase in the fluorescence lifetime ($\tau_\varphi = 2.61$ ns; $\tau_m = 2.73$ ns), compared to that of EGFP ($\tau_\varphi = 2.29$ ns; $\tau_m = 2.41$ ns). As expected, the low QY of SGFP2(T65G) was associated with a much shorter lifetime ($\tau_\varphi = 1.30$ ns; $\tau_m = 1.51$ ns). Due to the absence of a modulated UV excitation source in our FLIM system, we were unable to measure BFP lifetimes by frequency domain FLIM. Instead, time-correlated single-photon counting FLIM was used for the BFP variants (Table 3). For EBFP, an average lifetime ($\langle\tau\rangle$) of 1.42 ns was measured. Biexponential lifetime analysis indicated that the decay was multiexponential and mainly determined by a short lifetime component (0.86 ns). For SBFP1 and SBFP2, $\langle\tau\rangle$ was 2.07 and 2.35 ns, respectively. Biexponential lifetime analysis showed that the increase in average lifetime was caused by an increased contribution of the long lifetime component. For SBFP2, both lifetime components increased also. Like the GFP variants, the average fluorescence lifetime of the BFPs reflected the differences in QY.

Multicolor Confocal Imaging with SBFP2. Application of EBFP in confocal laser scanning microscopy has been limited because of the weak fluorescence and fast photobleaching of EBFP in combination with the low photon detection efficiency of confocal laser scanning microscopy. We tested whether our improved SBFP2 can be used for multicolor confocal microscopy in HeLa cells together with SGFP2 and the red fluorescent protein mCherry (*17*). To obtain distinct localization patterns from SBFP2, SGFP2 was targeted to the cytoplasm (SGFP2-cyt) and mCherry was targeted to the nucleus (mCherry-nuc). HeLa cells were imaged using confocal laser scanning microscopy with optimized filter sets to prevent cross talk between the fluorescent proteins (Figure S1 of the Supporting Information). Expression of SBFP2 yielded bright blue fluorescence well above cellular autofluorescence which was easily distinguished from SGFP2-cyt and mCherry-nuc fluorescence (Figure 5). We also attempted quadruple-color imaging with SBFP2, SCFP3A-golgi, mVenus-pm, and mCherry-nuc. To obtain distinct subcellular localization patterns, SCFP3A-golgi was targeted to the Golgi apparatus and excluded from the nucleus and mVenus-pm was targeted to the plasma membrane. The fluorescence spectra of SBFP2 and SCFP3A have considerable spectral overlap, and this increased the risk of bleed-through between SBFP2 and SCFP3A fluorescence (Figure S2 of the Supporting Information). Nevertheless, the fluorescence of all four fluorescent proteins was readily detected without significant bleed-through (Figure 6).

DISCUSSION

Introducing S72A, M153T, V163A, S175G, and A206K mutations into EGFP and EBFP improved the amount of correctly folded soluble fluorescent protein and increased the efficiency of chromophore formation. The resulting increase in fluorescence brightness was most profound in *E. coli*, in accordance with the inefficient folding of *A. victoria* (E)-VFPs in bacteria (*4*, *12*, *26*). Bacterial expression of SGFP2, taking into account the slightly reduced intrinsic brightness of the purified protein, yielded approximately 9-fold more fluorescence than expression of EGFP as a result of the combination of enhanced protein expression and maturation. For SBFP2, the increase in the level of protein expression and maturation was 4-fold compared to that of EBFP. Initially, the presence of mutation V68L resulted in suboptimal fluorescent proteins with reduced brightness. This effect was detrimental for SBFP1, which was highly sensitive to photobleaching and protein misfolding. No recovery of SBFP1 fluorescence was observed upon refolding in vitro. For SGFP1, however, in vitro refolding was fastest and most efficient of all GFP variants. Similar effects of the V68L mutation were observed when this mutation was inserted into YFP and CFP variants (*15*).

The increase in brightness of mammalian cells expressing one of the SGFP variants or SBFP2 was less pronounced,

Table 3: Fluorescence Lifetimes of GFP and BFP Variants[a]

	Frequency-Domain FLIM		
	τ_φ	τ_m	n
EGFP	2.29 ± 0.03	2.41 ± 0.03	8
SGFP1	2.42 ± 0.03	2.54 ± 0.02	8
SGFP2	2.61 ± 0.02	2.73 ± 0.02	8
SGFP2(206A)	2.64 ± 0.02	2.72 ± 0.02	8
SGFP2(E222Q)	2.08 ± 0.04	2.58 ± 0.06	8
SGFP2(T65G)	1.30 ± 0.02	1.51 ± 0.03	8
EGFP[b]	2.36 ± 0.06	2.42 ± 0.03	

	Time Domain FLIM							
	$\langle\tau\rangle$	χ^2	τ_1	α_1	τ_2	α_2	χ^2	n
EBFP	1.42 ± 0.01	7.6	0.86 ± 0.02	0.81 ± 0.01	2.24 ± 0.06	0.19 ± 0.01	1.6	3
SBFP1[c]	2.07 ± 0.01	3.1	0.85 ± 0.01	0.44 ± 0.01	2.35 ± 0.01	0.56 ± 0.01	2.0	2
SBFP2	2.35 ± 0.03	3.8	1.13 ± 0.05	0.43 ± 0.03	2.69 ± 0.02	0.57 ± 0.03	1.3	4

[a] Fluorescent proteins were expressed in mammalian cells. Fluorescence lifetimes are the mean average ± the standard deviation. [b] From ref *37*. [c] For SBFP1, purified protein was used for fluorescence lifetime measurements, due to the low expression levels in mammalian cells.

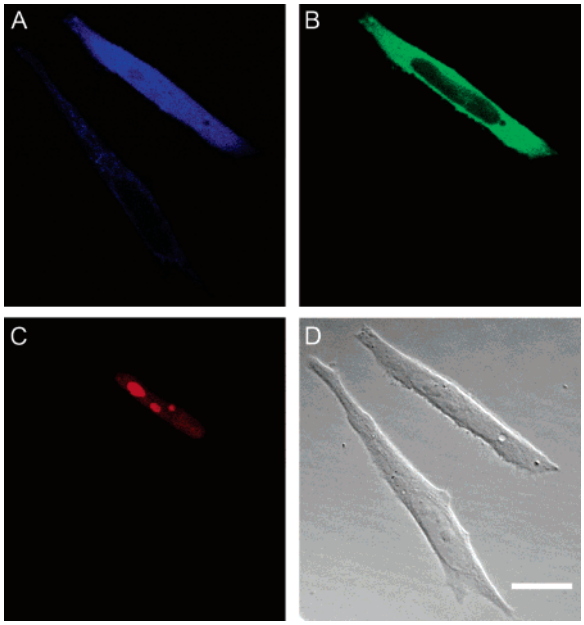

FIGURE 5: Triple-color confocal imaging with SBFP2, SGFP2, and mCherry. Fluorescence micrographs of a HeLa cell expressing SBFP2 (A), SGFP2-cyt (B), and mCherry-nuc (C). (D) DIC micrograph showing the presence of a transfected and a nontransfected cell. The scale bar is 20 μm.

presumably because protein expression and maturation of EGFP and EBFP were already relatively efficient. Mammalian cells have chaperone proteins which facilitate protein folding in mammalian cells, reducing the necessity of folding mutations (*26*). Comparing the brightness of mammalian cells expressing SGFP2 or EGFP with the intrinsic brightness of purified protein implied a 2-fold improvement in the amount of correctly folded protein, likely reflecting improved folding and maturation characteristics (see Figure 2 and Table 2). The same comparison between cells expressing SBFP2 and EBFP suggested that the increased brightness of cells expressing SBFP2 can be explained by the increase in intrinsic brightness and did not necessarily involve improved protein folding or maturation characteristics, even though the latter improvements were observed during the in vitro protein folding assays.

Introduction of the folding mutations in SGFP2 resulted in partial chromophore protonation. Because the protonated

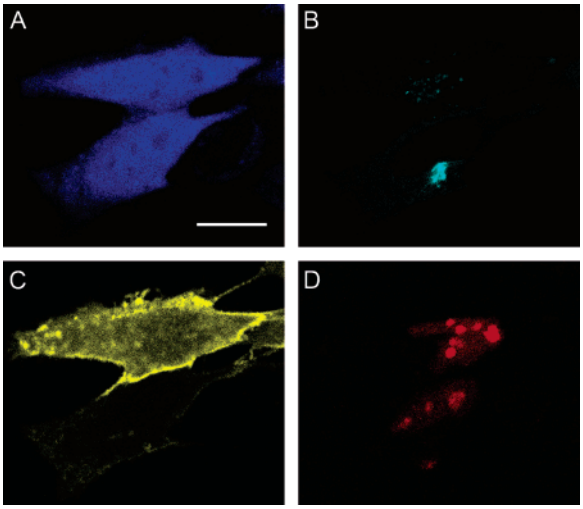

FIGURE 6: Quadruple-color confocal imaging with SBFP2, SCFP3A, mVenus, and mCherry. Fluorescence micrographs of HeLa cells expressing SBFP2 (A), SCFP3A-golgi (B), mVenus-pm (C), and mCherry-nuc (D). The scale bar is 20 μm.

chromophore is not excited at 488 nm, this resulted in a decrease in intrinsic brightness. We tested two mutations, E222Q and T65G, which effectively prevented chromophore protonation in SGFP2. Mutation E222Q, however, severely reduced the rate of chromophore formation in bacteria and in vitro. This was in accordance with a recent study conducted by Sniegowski and co-workers (*32*), who found that at pH 7 chromophore formation in EGFP(E222Q) was attenuated approximately 30-fold. Alternatively, for SGFP2-(T65G), the absorbance spectrum was red-shifted, and its shape resembled closely that of the yellow fluorescent protein. Similar changes have been observed for the GFP variant GFPmut3, which contains mutations S65G and S72A (*4*). Although the molar extinction of SGFP2(T65G) was enhanced, this was counteracted by a decrease in QY, and therefore, SGFP2 and SGFP2(T65G) were expected to be more or less equally bright. Bacteria expressing SGFP2, however, became much more fluorescent than those expressing SGFP2(T65G). To a certain extent, this decrease was caused by less efficient excitation of SGFP2(T65G), given its red-shifted absorbance. In addition, the SGFP2(T65G) fluorescence could have been partially quenched due to its

high pK_a. In conclusion, chromophore protonation of SGFP2 could be prevented, but at the cost of reducing the QY or speed of chromophore formation.

Despite the partial chromophore protonation, we believe that SGFP2 is superior to EGFP because of its improved protein folding, increased QY and fluorescence lifetime, and increased photostability. The improvements in protein folding and chromophore maturation surpass the effect of chromophore protonation. The increased fluorescence lifetime makes SGFP2 more suitable for FLIM measurements, especially for use as a donor in FRET applications, as the longer lifetime will enable larger lifetime changes due to FRET. In addition, SGFP2 and SGFP2(T65G) should make an excellent GFP pair for dual-lifetime imaging because of their large lifetime difference (*35*−*37*). Nonetheless, as abolishing chromophore protonation in SGFP2 might result in even brighter GFP variants, it will be interesting to try other means of eliminating chromophore protonation, for example, high-throughput random mutagenesis methods like molecular evolution (*33*) or iterative somatic hypermutation (*34*).

The increased QY and photostability of SBFP2 are important steps toward bright blue fluorescent proteins. Strikingly, the QY of the original blue fluorescent variant P4-3 (*9*) is close to that of SBFP2. We are therefore inclined to suggest that the low QY of EBFP might be related to the S65T mutation. Photobleaching limits the number of images that can be recorded during time-lapse imaging. Because SGFP2 and SBFP2 bleach 2-fold slower than EGFP and EBFP, the number of images that can be collected before fading of the fluorescence should increase. In addition, the increased brightness of SGFP2 and SBFP2 should allow a reduction of the excitation light intensity, thereby further reducing bleaching. The combination of increased photostability and brightness should permit 2.6- and 7.4-fold longer imaging of SGFP2 and SBFP2 than of EGFP and EBFP, respectively.

During revision of the manuscript, another optimized BFP variant, Azurite (*38*), was published. Azurite lacks the T65S mutation and contains two novel mutations, V150I and V224R, compared to EBFP or SBFP2. Azurite displayed an increased QY and photostability. The intrinsic brightness of Azurite (based on its published QY and extinction coefficient) is slightly lower (10%) than that of SBFP2. Because the codon usage of Azurite is markedly different from that of EBFP or SBFP2 (not mammalian-codon optimized), it is not possible to directly compare folding efficiencies in cells. Whether V150I and V224R mutations could further improve SBFP2 is currently under investigation.

This study, combined with the previous work (*15*), demonstrates that folding mutations generally improve protein folding of all VFP color variants derived from *A. victoria* GFP. Together, these improved SVFP variants constitute a new generation of strongly enhanced fluorescent proteins. The benefits of these new variants are most pronounced in bacteria. With the demonstration of quadruple-color confocal microscopy, we show that the SVFPs can make a valuable contribution to cell−biological applications, also in mammalian cell systems.

ACKNOWLEDGMENT

We thank Dr. A. Miyawaki (Brain Science Institute, RIKEN, Saitama, Japan) for the pCS2+ Venus plasmid, Dr. R. Y. Tsien (Howard Hughes Medical Institute, University of California at San Diego, La Jolla, CA) for the cDNA encoding mCherry, and Dr. T. Levine (Institute of Ophthalmology, Department of Cell Biology, University College London, London, U.K.) for making available the plasmid pBGPa containing the PH domain of OSBP. We thank B. Hooibrink (FACS facility AMC, Amsterdam, The Netherlands) for assistance with flow cytometry, Dr. A. Los (Division of Cellular Biochemistry, Dutch Cancer Institute, Amsterdam, The Netherlands) for providing the Swiss 3T3 cells, and Dr. R. K. P. Benninger (Department of Molecular Physiology and Biophysics, Vanderbilt University Medical Center, Nashville, TN) for critically reading the manuscript.

SUPPORTING INFORMATION AVAILABLE

Oligonucleotides used for site-directed mutagenesis (Table S1) and spectra and filter sets used for multicolor confocal imaging (Figures S1 and S2). This material is available free of charge via the Internet at http://pubs.acs.org.

REFERENCES

1. Prasher, D. C., Eckenrode, V. K., Ward, W. W., Prendergast, F. G., and Cormier, M. J. (1992) Primary structure of the *Aequorea victoria* green-fluorescent protein, *Gene 111*, 229−233.
2. Tsien, R. Y. (1998) The green fluorescent protein, *Annu. Rev. Biochem. 67*, 509−544.
3. Chudakov, D. M., Lukyanov, S., and Lukyanov, K. A. (2005) Fluorescent proteins as a toolkit for in vivo imaging, *Trends Biotechnol. 23*, 605−613.
4. Cormack, B. P., Valdivia, R. H., and Falkow, S. (1996) FACS-optimized mutants of the green fluorescent protein (GFP), *Gene 173*, 33−38.
5. Patterson, G. H., Knobel, S. M., Sharif, W. D., Kain, S. R., and Piston, D. W. (1997) Use of the green fluorescent protein and its mutants in quantitative fluorescence microscopy, *Biophys. J. 73*, 2782−2790.
6. Reid, B. G., and Flynn, G. C. (1997) Chromophore formation in green fluorescent protein, *Biochemistry 36*, 6786−6791.
7. Heim, R., Prasher, D. C., and Tsien, R. Y. (1994) Wavelength mutations and posttranslational autoxidation of green fluorescent protein, *Proc. Natl. Acad. Sci. U.S.A. 91*, 12501−12504.
8. Rizzuto, R., Brini, M., De Giorgi, F., Rossi, R., Heim, R., Tsien, R. Y., and Pozzan, T. (1996) Double labelling of subcellular structures with organelle-targeted GFP mutants in vivo, *Curr. Biol. 6*, 183−188.
9. Heim, R., and Tsien, R. Y. (1996) Engineering green fluorescent protein for improved brightness, longer wavelengths and fluorescence resonance energy transfer, *Curr. Biol. 6*, 178−182.
10. Yang, T. T., Sinai, P., Green, G., Kitts, P. A., Chen, Y. T., Lybarger, L., Chervenak, R., Patterson, G. H., Piston, D. W., and Kain, S. R. (1998) Improved fluorescence and dual color detection with enhanced blue and green variants of the green fluorescent protein, *J. Biol. Chem. 273*, 8212−8216.
11. Cubitt, A. B., Woollenweber, L. A., and Heim, R. (1999) Understanding structure-function relationships in the *Aequorea victoria* green fluorescent protein, *Methods Cell Biol. 58*, 19−30.
12. Siemering, K. R., Golbik, R., Sever, R., and Haseloff, J. (1996) Mutations that suppress the thermosensitivity of green fluorescent protein, *Curr. Biol. 6*, 1653−1663.
13. Fukuda, H., Arai, M., and Kuwajima, K. (2000) Folding of green fluorescent protein and the cycle3 mutant, *Biochemistry 39*, 12025−12032.
14. Zacharias, D. A., Violin, J. D., Newton, A. C., and Tsien, R. Y. (2002) Partitioning of lipid-modified monomeric GFPs into membrane microdomains of live cells, *Science 296*, 913−916.
15. Kremers, G. J., Goedhart, J., van Munster, E. B., and Gadella, T. W., Jr. (2006) Cyan and yellow super fluorescent proteins with

improved brightness, protein folding, and FRET Forster radius, *Biochemistry 45*, 6570−6580.
16. Nagai, T., Ibata, K., Park, E. S., Kubota, M., Mikoshiba, K., and Miyawaki, A. (2002) A variant of yellow fluorescent protein with fast and efficient maturation for cell-biological applications, *Nat. Biotechnol. 20*, 87−90.
17. Shaner, N. C., Campbell, R. E., Steinbach, P. A., Giepmans, B. N., Palmer, A. E., and Tsien, R. Y. (2004) Improved monomeric red, orange and yellow fluorescent proteins derived from *Discosoma* sp. red fluorescent protein, *Nat. Biotechnol. 22*, 1567−1572.
18. Levine, T. P., and Munro, S. (2002) Targeting of Golgi-specific pleckstrin homology domains involves both PtdIns 4-kinase-dependent and -independent components, *Curr. Biol. 12*, 695−704.
19. Varnai, P., and Balla, T. (1998) Visualization of phosphoinositides that bind pleckstrin homology domains: Calcium- and agonist-induced dynamic changes and relationship to myo-[^{3}H]inositol-labeled phosphoinositide pools, *J. Cell Biol. 143*, 501−510.
20. Stauffer, T. P., Ahn, S., and Meyer, T. (1998) Receptor-induced transient reduction in plasma membrane PtdIns(4,5)P2 concentration monitored in living cells, *Curr. Biol. 8*, 343−346.
21. Velapoldi, R. A., and Tonnesen, H. H. (2004) Corrected emission spectra and quantum yields for a series of fluorescent compounds in the visible spectral region, *J. Fluoresc. 14*, 465−472.
22. van Munster, E. B., and Gadella, T. W., Jr. (2004) phiFLIM: A new method to avoid aliasing in frequency-domain fluorescence lifetime imaging microscopy, *J. Microsc. 213*, 29−38.
23. van Munster, E. B., and Gadella, T. W., Jr. (2004) Suppression of photobleaching-induced artifacts in frequency-domain FLIM by permutation of the recording order, *Cytometry 58A*, 185−194.
24. Press, W. H., Teukolky, S. A., Vetterling, W. T., and Flannery, B. P. (1992) *Numerical Recipes in C*, 2nd ed., Cambridge University Press, Cambridge, U.K.
25. Sacchetti, A., Cappetti, V., Marra, P., Dell'Arciprete, R., El Sewedy, T., Crescenzi, C., and Alberti, S. (2001) Green fluorescent protein variants fold differentially in prokaryotic and eukaryotic cells, *J. Cell. Biochem. 36* (Suppl.), 117−128.
26. Chang, H. C., Kaiser, C. M., Hartl, F. U., and Barral, J. M. (2005) De novo folding of GFP fusion proteins: High efficiency in eukaryotes but not in bacteria, *J. Mol. Biol. 353*, 397−409.
27. Peyker, A., Rocks, O., and Bastiaens, P. I. (2005) Imaging activation of two Ras isoforms simultaneously in a single cell, *ChemBioChem 6*, 78−85.
28. Gadella, T. W., Jr., Jovin, T. M., and Clegg, R. M. (1993) Fluorescence lifetime imaging microscopy (FLIM): Spatial resolution of microstructures on the nanosecond time scale, *Biophys. Chem. 48*, 221−239.
29. Gadella, T. W., Jr., and Jovin, T. M. (1995) Oligomerization of epidermal growth factor receptors on A431 cells studied by time-resolved fluorescence imaging microscopy. A stereochemical model for tyrosine kinase receptor activation, *J. Cell Biol. 129*, 1543−1558.
30. Bastiaens, P. I., and Squire, A. (1999) Fluorescence lifetime imaging microscopy: Spatial resolution of biochemical processes in the cell, *Trends Cell Biol. 9*, 48−52.
31. Wouters, F. S., and Bastiaens, P. I. (1999) Fluorescence lifetime imaging of receptor tyrosine kinase activity in cells, *Curr. Biol. 9*, 1127−1130.
32. Sniegowski, J. A., Lappe, J. W., Patel, H. N., Huffman, H. A., and Wachter, R. M. (2005) Base catalysis of chromophore formation in Arg96 and Glu222 variants of green fluorescent protein, *J. Biol. Chem. 280*, 26248−26255.
33. Nguyen, A. W., and Daugherty, P. S. (2005) Evolutionary optimization of fluorescent proteins for intracellular FRET, *Nat. Biotechnol. 23*, 355−360.
34. Wang, L., Jackson, W. C., Steinbach, P. A., and Tsien, R. Y. (2004) Evolution of new nonantibody proteins via iterative somatic hypermutation, *Proc. Natl. Acad. Sci. U.S.A. 101*, 16745−16749.
35. Ganesan, S., Ameer-Beg, S. M., Ng, T. T., Vojnovic, B., and Wouters, F. S. (2006) A dark yellow fluorescent protein (YFP)-based resonance energy-accepting chromoprotein (REACh) for Forster resonance energy transfer with GFP, *Proc. Natl. Acad. Sci. U.S.A. 103*, 4089−4094.
36. Scruggs, A. W., Flores, C. L., Wachter, R., and Woodbury, N. W. (2005) Development and Characterization of Green Fluorescent Protein Mutants with Altered Lifetimes, *Biochemistry 44*, 13377−13384.
37. Pepperkok, R., Squire, A., Geley, S., and Bastiaens, P. I. (1999) Simultaneous detection of multiple green fluorescent proteins in live cells by fluorescence lifetime imaging microscopy, *Curr. Biol. 9*, 269−272.
38. Mena, M. A., Treynor, T. P., Mayo, S. L., and Daugherty, P. S. (2006) Blue fluorescent proteins with enhanced brightness and photostability from a structurally targeted library, *Nat. Biotechnol. 24*, 1569−1571.
39. Patterson, G., Day, R. N., and Piston, D. (2001) Fluorescent protein spectra, *J. Cell Sci. 114*, 837−838.
40. Sawano, A., and Miyawaki, A. (2000) Directed evolution of green fluorescent protein by a new versatile PCR strategy for site-directed and semi-random mutagenesis, *Nucleic Acids Res. 28*, E78.

BI0622874